Zirconia/hydroxyapatite (80/20) scaffold repair in critical size calvarial defect increased FGF-2, osteocalcin and OPG immunostaining and IL-10 levels

Vasconcelos, R.C.; Ferreira, C.; Araujo, E.M. de; Motta, F.; Bomio, M.; Araujo, R.F. de; ... ; Araujo, A.A. de

Am J Transl Res 2020;12(6):2439-2450
www.ajtr.org /ISSN:1943-8141/AJTR0104182

Original Article

Zirconia/hydroxyapatite (80/20) scaffold repair in critical size calvarial defect increased FGF-2, osteocalcin and OPG immunostaining and IL-10 levels

Roseane Carvalho Vasconcelos[1], Camyla Ferreira[2], Eduarda Medeiros de Araújo[2], Fabiana Motta[2], Mauricio Bomio[2], Raimundo Fernandes de Araújo Júnior[3], Daniel Felipe Fernandes Paiva[4], Flavia Q Pirih[5], Jose Sandro Pereira da Silva[6], Alan B Chan[7], Luis J Cruz[8], Makiko Ishii[9], Caroline Addison Carvalho Xavier de Medeiros[10], Gerlane Coelho Bernardo Guerra[11], Aurigena Antunes de Araújo[12]

[1]Postgraduate Program in Health Sciences, UFRN, Department of Biophysics and Pharmacology, Federal University of Rio Grande Norte, Natal, RN, Brazil; [2]Postgraduate Program in Material Engineering, UFRN, Department of Material Engineering, Federal University of Rio Grande Norte, Natal, RN, Brazil; [3]Postgraduate Program in Health Sciences, Postgraduate Program in Functional and Structural Biology, UFRN, Department of Morphology, Federal University of Rio Grande Norte, Natal, RN, Brazil; [4]Department of Dentistry, Federal University of Rio Grande Norte, Natal, RN, Brazil; [5]School of Dentistry, University of California-Los Angeles (UCLA), USA; [6]Postgraduate Program in Dentistry Sciences, Department of Dentistry, Federal University of Rio Grande Norte, Natal, RN, Brazil; [7]Percuros B.V, 2333 CL Leiden, The Netherlands; [8]Translational Nanobiomaterials and Imaging, Department of Radiology, Leiden University Medical Center, 2333 ZA Leiden, The Netherlands; [9]Department of Periodontology, Meikai University, Saitama, Japan; [10]Postgraduate Program in Biological Science, Postgraduate Program in RENORBIO, Department of Biophysical and Pharmacology, Federal University of Rio Grande Norte, Natal, RN, Brazil; [11]Postgraduate Program in Biological Sciences, Postgraduate Program in Pharmaceutical Sciences, Department of Biophysical and Pharmacology, Federal University of Rio Grande Norte, Natal, RN, Brazil; [12]Visiting Research in UCLA, Postgraduate Program in Dentistry Sciences, Postgraduate Program in Pharmaceutical Sciences, Department of Biophysical and Pharmacology, Federal University of Rio Grande Norte, Natal, RN, Brazil

Received October 29, 2019; Accepted April 13, 2020; Epub June 15, 2020; Published June 30, 2020

Abstract: The aim of this study was to characterize and evaluate zirconia/hydroxyapatite in a critical size calvarial defect model in rats. Zirconia/hydroxyapatite (80/20) scaffold was characterized by X-ray diffraction (XRD) and Scanning Electron Microscopy (SEM). Critical size (8 mm) calvarial defects were created in wistar rats (n=48) and divided into four groups (90 days): G0 Group: positive control; G1 Group: hydroxyapatite; G2 Group: Zirconia; G3 Group: Zirconia/hydroxyapatite (80/20). Calvaria were subjected to Micro CT, histological and immunohistochemical analyses (RANK, RANKL, OPG, osteocalcin and FGF-2). IL-1 beta, IL-10 and TNF-alpha levels were analyzed by Elisa Immunoassay. The XRD analysis confirmed the formation of a crystalline structure and SEM showed the presence of regions corresponding to Zirconia and Hydroxyapatite. The Micro CT showed increased bone volume (BV/TV) and bone mineral density (BMD) in the G3 group ($P<0.05$). In addition, discrete periosteal bone formation was found at the interface of the defect edge and the external surface of the scaffold in the G3 group, showing osteocytes inside and osteoblasts ($P<0.05$) with scarce mononuclear inflammatory cells ($P<0.01$) in the central region of the defect. The immunostaining was moderate for RANKL, Osteocalcin and FGF-2 in the G3 group ($P<0.5$), while it was intense for OPG ($P<0.001$). IL-1 beta levels were decreased and IL-10 levels increased ($P<0.05$). Zirconia/hydroxyapatite (80/20) scaffold repair in critical size calvarial defects increased bone density, osteoblast and osteoclast cell numbers, FGF-2, osteocalcin and OPG immunostaining and IL-10 levels.

Keywords: Zirconia, hydroxyapatite, scaffold, calvaria defect

Introduction

Bone lesions often occur in the population, largely causing significant bone loss [1, 2]. The development of biomaterials has led to discovering new products to replace injured tissue. One of the options has been the use of biological frameworks to assist the wound healing

process, alone or in combination with other procedures which stimulate repair [1, 3].

Hydroxyapatite (HA) is one of the most studied compounds used for clinical purposes, especially because it is a mineral component with more prominence in bone and teeth formation. HA has been utilized to correct craniomaxillofacial defects, trauma, congenital deformities and also in aesthetic medicine in the correction of inherently deficient areas of the facial skeleton [4]. HA has good bone conductivity and resorption speed, and it is important to highlight that this material stimulates osteogenesis in the area in contact with bone [5].

The main property of biomaterials used for bone grafting is osteoconduction. Osteoconduction is the ability of a material to serve as a framework for bone cell migration. Experiments in goats [6] have confirmed the osteoconductive capacity of nanohydroxyapatite in healing bone defects. The osteoconductive effect directly depends on the porosity of the material, enabling migration of osteoblasts to the interior, making an integration between surfaces viable.

Liao et al. emphasized that HA composites are osteoconductive, biocompatible and have similar minerals to bones; however, the authors emphasize that the fragility of this material should be taken into consideration [8]. Conz et al. stated that one of the main challenges of bone graft biomaterials used for bone reconstruction is to increase the strength of HA composites to withstand the forces applied during surgical procedures [9].

Ceramics are among the materials with resistance to mechanical forces [7]. Piconi C and Maccauro point out that ceramics such as zirconia have good chemical and dimensional stability, mechanical strength and toughness, and therefore have generated interest as suitable biomaterials for bone graft substitutes [10]. Even though, zirconia has many excellent properties, the authors point out that there is a need to stabilize porcelains in order to ensure its correct production [10]. Therefore, taking into consideration the qualities and weaknesses of hydroxyapatite and zirconia, this study aims to characterize and evaluate the zirconia/hydroxyapatite scaffold on a calvarial defect experimental model.

Materials and methods

Materials

The materials used to obtain the composites were 8 mol% of yttria-stabilized zirconia (YSZ) (TOSOH CORPORATION) with batch number Z802964P and hydroxyapatite (HAp). The hydroxyapatite was synthesized by the sol-gel method with precursors such as phosphoric acid (H_3PO_4, Vetec, 85%), calcium nitrate tetrahydrate ($Ca(NO_3)_2{\cdot}4H_2O$, Vetec, 99%) and distilled water.

Obtaining zirconia/hydroxyapatite (80/20)

The Zirconia/Hydroxyapatite (80/20) composite was weighed on a digital scale, and the homogenization was carried out using an ultrasonic tip with ethyl alcohol. The composition was quickly poured into a hot vessel and put into the oven for drying to avoid phase separation in the process. When dried, the composite was macerated and sent for characterization. Hydroxyapatite, commercial zirconia powders and YSZ/HAp composites were characterized by X-ray diffraction (XRD, 40 kV, XRD-7000, SHIMADZU), Vickers microhardness test (FM-810, Futuretech) and Scanning Electron Microscopy (SEM, HITACHI 3M-3000).

X-ray diffraction (XRD)

The studies were performed on a SHIMADZU model XRD-7000, with an angular range of 20° to 120°, at a step of 0.02° and a speed of 1°/min, with the equipment adjusted to 40 kV. XRD patterns provide information about the chemical composition and structure of crystalline materials. XRD is the only technique used for qualitative and quantitative analysis.

Scanning electron microscopy (SEM)

SEM analysis was performed on HITACHI equipment (model 3M-3000) to analyze specimen indentation and measure the semi-diagonal crack sizes of the indentation marks.

Experimental model in animals

The experimental protocols were performed according to the guidelines approved by the Animal Research Ethics Committee (CEUA)/UFRN, protocol number 022020/2017. The

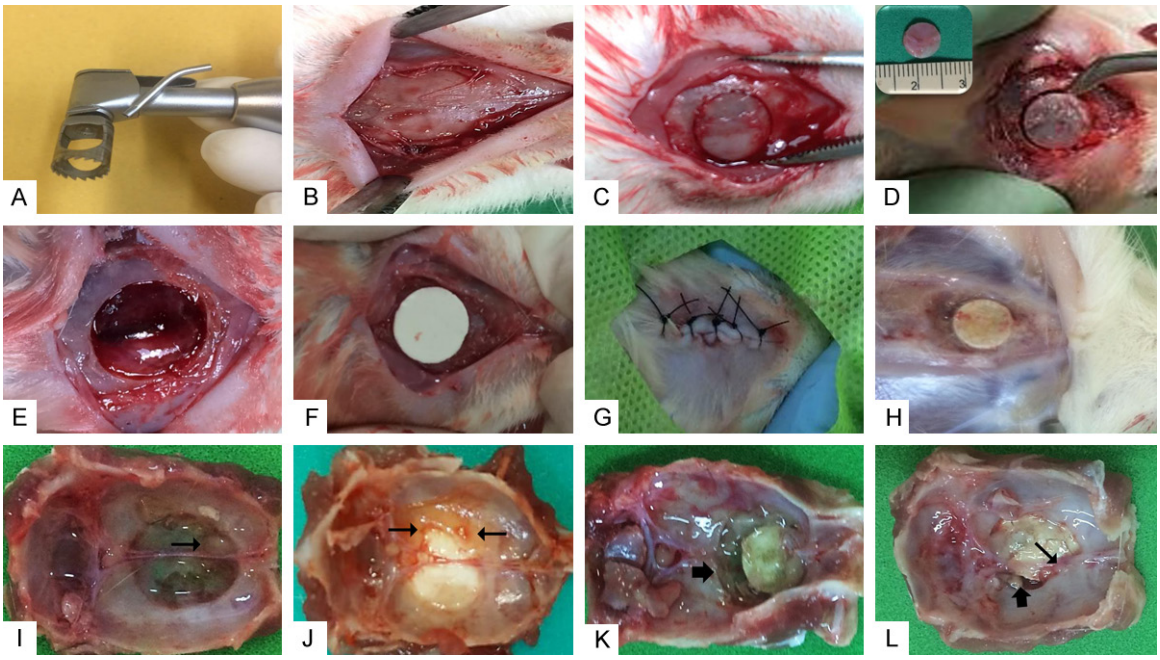

Figure 1. Surgical procedure for implantation of biomaterials. (A) Trephine drill, measuring 8 mm in diameter, used for drilling the defect. (B) Integral incision, soft tissue disruption, exposure of calvaria bone. (C) Critical bone defect in calvaria. (D) Removal of bone fragment from defect area measuring 8 mm in diameter as shown in detail. (E) Defect area with exposure of the integra after removal of the calvaria bone. (F) Implantation of biomaterial in defect according to group. (G) Soft tissue approach and simple suture. (H) Moment of euthanasia showing biomaterial filling the defect after 12 weeks. (I) G0 Group specimen showing defect area filled with fibrous connective tissue and small projection of formed bone (arrow). (J) G1 Group specimen showing bone formation at the edge of the defect in contact with the biomaterial (arrows). (K) G2 Group showing bone resorption area adjacent to the implanted biomaterial (arrows). (L) G3 Group in which bone formation area is observed in contact with the implanted composite (narrow arrow) and slight bone resorption (wide arrow). G0 Group: Positive control critical defect (D) filled with blood clot; G1 Group: Critical defect filled with hydroxyapatite (H) scaffold; G2 Group: Critical defect filled with zirconia (YSZ) scaffold; G3 Group: Critical defect filled with zirconia/hydroxyapatite (80/20) scaffold.

Institutional Animal Care and Use Committees (IACUCs) located at UFRN, Natal/Brazil, and the Animal Research: Reporting *in vivo* Experiments ARRIVE guidelines [12] and protocols were approved and followed. Adult Male Wistar rats, (*Rattus novergicus* albinus, Wistar), weighing approximately 300 g, were obtained from the Laboratory of the Department of Pharmacology of the Federal University of Rio Grande do Norte. Rats were distributed into the following four groups: Group 0: Positive control: Critical defect (D) filled with blood clot. Group 1: Critical defect filled with Hydroxyapatite (H) scaffold; Group 2: Critical defect filled with zirconia (YSZ) scaffold; and Group 3: Critical defect filled with Zirconia/Hydroxyapatite (80/20) scaffold. Each group consisted of 12 animals: four animals were used for morphological and immunohistochemical analysis, four for Micro-CT, and four for cytokine analysis (IL-1, IL-10, TNF) by ELISA immunoassay.

Rats were anesthetized with a combination of 10% ketamine hydrochloride (80 mg/kg) and 2% xylazine hydrochloride (10 mg/kg), trichotomy and antisepsis of the integument with topical polivinilpirrolidona-iodo (PVPI), and then a rectilinear incision of approximately 2 cm in the integument of the median skull was performed to access the calvaria to create the rat critical size calvarial defect. The periosteum was laterally divulged and a bony defect measuring 8 mm in diameter was created in the central region of the calvaria utilizing a trephine drill, with constant saline irrigation. Then, the defect area was filled with the biomaterial corresponding to the study groups. Soft tissue was sutured with 4-0 nylon. (Shalon, Sao Paulo, Brazil) (**Figure 1**). The animals received feed and water *ad libitum* in the UFRN Department of Pharmacology for the entire period of the experiment (12 weeks). After this period, the animals

were euthanized using ketamine and xylazine hydrochloride overdose.

Micro-CT analysis

The maxilla was dissected and fixed with 4% paraformaldehyde in 0.1 M phosphate-buffered saline solution for 24 hours. Samples were scanned using a high-resolution micro-CT (SkyScan 1172, Sky-Scan N.V., Belgium) at an image resolution of 15 μm, with 70 kV and 148 μA x-ray source and 0.5 mm aluminum filter. Then three-dimensional (3D) image datasets were reconstructed from two-dimensional x-ray images using NRecon software (SkyScan N.V.), with processes including appropriate image correction steps including ring artifact correction, beam hardening correction and fine-tuning. After acquisition of the datasets, the images of samples were viewed and reoriented on each 3D plane with DataViewer software (SkyScan N.V.) to align the palatal defects parallel to the transaxial plane to minimize analysis errors [13].

A 3D volumetric analysis was performed using CTAn software (SkyScan N.V.). Images were performed with DOLPHIN@ software (Navantis, Toronto, CAN). All analyses were repeated at a separate time point by a single rater to ensure consistency of results. The region of interest was outlined with a transaxial sections in order to create a uniform, cylindrical-shaped volume of interest, which encloses the entire defect area. Grey threshold values were determined by approximating images to their true morphology. Bone volume (BV) and tissue volume (TV) were measured to calculate percent bone volume (BV/TV) of each graft site, and bone mineral density (BMD) was also calculated.

Histological analysis

Samples were processed by the Biosciences Morphology Laboratory-UFRN. Four samples (n=4) from each group were decalcified in 4.3% EDTA solution (pH 7.4) for five weeks. The defect region was sectioned in a transverse orientation and each side of the defect was embedded in paraffin. First, 4 μm-thick sections were obtained and stained with hematoxylin and eosin. Histological sections were blindly analyzed by a pathologist by conventional light microscope (Olimpus®CH2, Olimpus Optical Co. Ltd, Japan).

The following histomorphological events, adapted from Prantel (2007), were evaluated [14]: (a) Inflammation: (score 0) absence of inflammatory cells; (score 1) weak presence of inflammatory cells; (score 2) moderate presence of inflammatory cells; (score 3) intense presence of inflammatory cells; (b) Bone Cell Types: Osteoblast: (score 0) absence; and (score 1) presence; Osteocyte: (score 0) absence; and (score 1) presence; and Osteoclasts: (score 0) absence; and (score 1) presence.

Immunohistochemical analysis

3 μm-thick histological sections mounted on glass slides previously prepared with 3-aminopropyltriethoxy silane-based adhesives (Sigma Chemical Co, St. Louis, MO, USA) were subjected to the LSAB immunoperoxidase method using the following primary anti-human antibodies: RANK (1:400), anti-RANKL (1:400), anti-OPG (1:400), anti-osteocalcin (1:400) and anti-FGF-2 (1:400) (Santa Cruz Biothecnology, Miami, USA). Immunoreactivity was analyzed by scores assigned according to the percentage of cellular labeling [15]. Score 0: immunostaining absence; Score 1: weak labeling (<25% positive cells); score 2: moderate labeling (25% to 50% positive cells) and score 3: intense immunostaining (>50% positive cells).

Detection of IL-1β and TNF-α by elisa immunoassay

Rat calvaria (*n*=4/group) were stored at -70°C, then IL-1β levels (detection range: 62.5-4000 pg/mL; lower detection limit: 12.5 ng/mL of recombinant mouse IL-1β), IL-10 levels (detection range: 62.5-4000 pg/mL; lower detection limit: 12.5 ng/mL of recombinant mouse IL-1β) and TNF-α (detection range: 62.5-4000 pg/mL; lower limit of detection: 50 ng/mL mouse TNF-α recombinant) were determined using commercial ELISA kits (R&D Systems, Minneapolis, MN, USA) according to the manufacturer's protocol. All samples were measured at 490 nm.

Statistical analysis

The data are presented as means ± standard error of the mean or as medians, when appropriate. One-way analysis of variance (ANOVA) followed by the Bonferroni test was used to compare significance among groups. The Kruskal-Wallis test followed by Dunn's test was

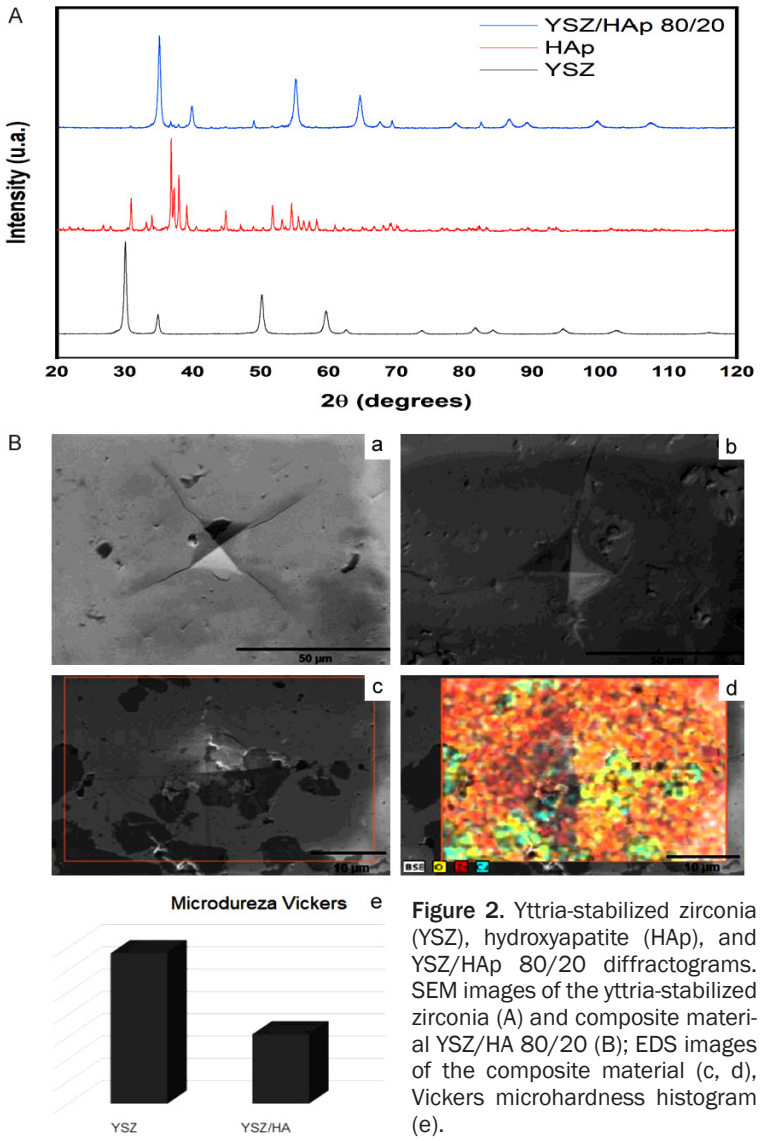

Figure 2. Yttria-stabilized zirconia (YSZ), hydroxyapatite (HAp), and YSZ/HAp 80/20 diffractograms. SEM images of the yttria-stabilized zirconia (A) and composite material YSZ/HA 80/20 (B); EDS images of the composite material (c, d), Vickers microhardness histogram (e).

used to compare medians. Data were averaged per each group and compared using a Student's t-test for radiographic linear and volumetric bone loss. A *p*-value of $P \leq 0.05$ indicated statistical significance (GraphPad Prism 5.0 Software, La Jolla, CA, USA).

Results

XRD analysis

Figure 2 shows the diffractograms of the yttria-stabilized zirconia (YSZ), hydroxyapatite (HAp) and composite material (YSZ/HAp) samples. The presence of yttria-stabilized zirconia and hydroxyapatite were identified with the aid of ICSD card No. 075316 and ICSD No. 26205, respectively. It is possible to observe the presence of the yttria-stabilized zirconia phase with discrete hydroxyapatite peaks for YSZ/HAp (80/20) composite material, **Figure 1**.

SEM analysis

Figure 2B shows images of yttria-stabilized zirconia samples (a), and the composite material containing 20% hydroxyapatite in its composition (b). The entire metallographic process was performed to prepare the samples with sanding and polishing for visualization in SEM. It is possible to observe the indentations resulting from the Vickers microhardness analysis through the scanning electron microscopy technique, **Figure 2B** (a) and (b), respectively.

A darker or lighter region is identified according to the presence of hydroxyapatite in the sample based on the general qualitative analysis of the elements (**Figure 2B** (c and d)). The lightest region is the composition with the yttria-stabilized zirconia and the darkest region is rich in hydroxyapatite [**Figure 2B** (d) zirconia in red and hydroxyapatite in blue]. **Figure 2B** (e) represents the Vickers microhardness difference in the zirconia and composite material samples.

Micro CT

Micro-CT has been considered the gold standard for assessing trabecular bone microarchitecture. Quantitative analyses were performed by comparing the bone volume of specimens from the rats with HA, zirconia, or Zirconia/HA (80/20) Scaffolds. Increased bone volume (BV/TV) and bone mineral density (BMD) percentages were showed in G1, G2 and G3 groups ($P<0.05$, **Figure 3**). However, the HA scaffold group (G1 group) showed fractures and soft tissue invasion. The zirconia scaffold (G2 group)

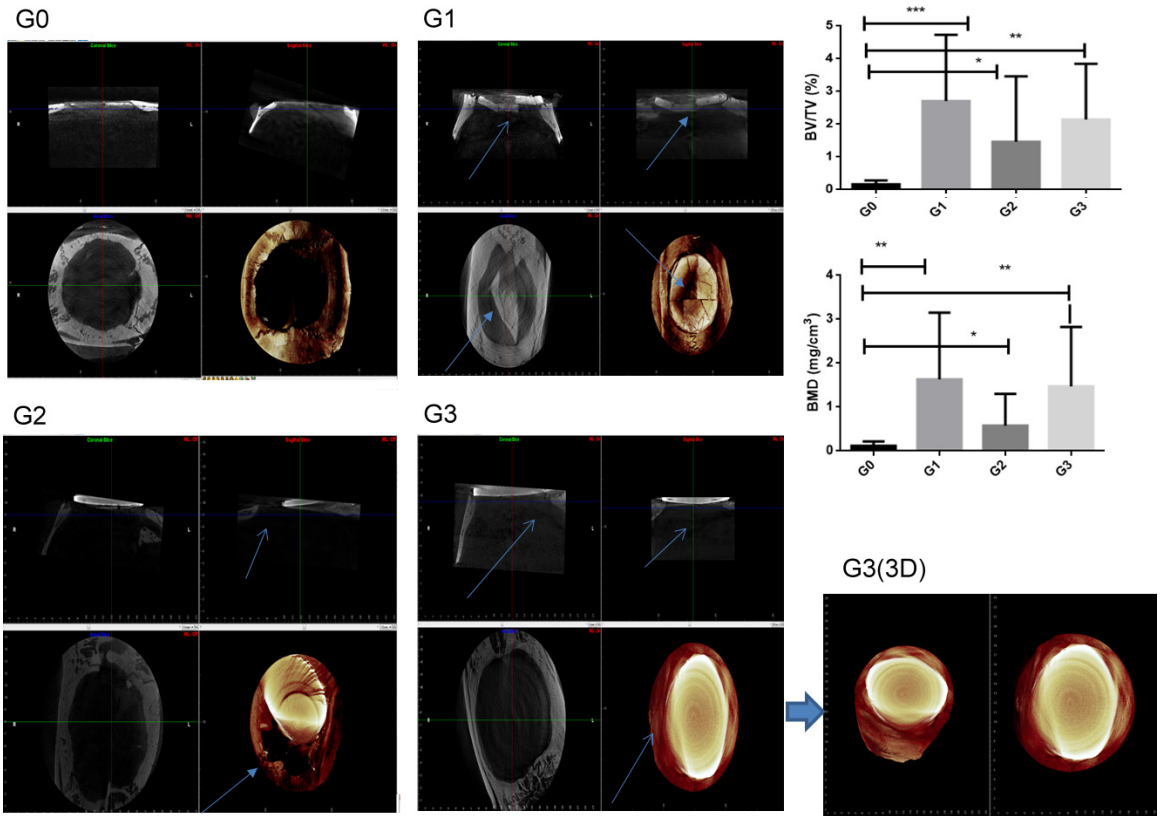

Figure 3. Micro CT analysis. Sargittal image; Transversal image, Coronal image and 3D (tridimensional) image. Percent bone volume (BV/TV) and bone mineral density (BMD), (ANOVA test followed by Bonferroni), (*P<0.05). G1 (arrow): Fracture of hydroxyapatite. G2 (arrow): No binding to zirconia-bone tissue. G3 (arrow): No fracture and bind between zirconia/hydroxyapatite (80/20) scaffold-bone tissue.

did not show osteointegration with bone tissue. The image showed wound displacement, with soft tissue exposure. The zirconia/hydroxyapatite (80/20) scaffold (G3 group) showed no fracture, no soft tissue invasion, and osteointegration with bone tissue (**Figure 3**).

Histological analysis

For the G0 Group, discreet projections of new bone formation were observed with osteocytes inside. Focal areas showed a slight presence of osteoblasts in the periphery and absence of osteoclasts (P<0.001 compared to G2 group, **Figure 6**). Fibrous connective tissue by fibroblasts and scarce mononuclear inflammatory cells (P<0.05 compared to G2 group, **Figure 6**) fill the central area of the defect (**Figure 4A-D**).

In the G1 group (HA), internal filling of the connective tissue defect was partially inhibited by the implanted biomaterial and discreet bone formation exhibiting osteocytes and regions with osteoblastic paving was observed in the margin (P<0.01 compared to G2 group, **Figure 6**). There was also a slight mononuclear inflammatory infiltrate (P<0.01 compared to G2 group, **Figure 6**) and a slight presence of osteoclasts showing bone resorption in focal areas (**Figure 4E-H**).

In the G2 group, small bone fragments with irregular margins containing osteocytes were formed in the margin of the defect, but no osteoblasts were present. Bone trabeculae resorption by numerous osteoclasts were observed in some fields. Intense mononuclear inflammatory infiltrate permeating fibrous connective tissue and multinucleated giant cells were observed, showing an inflammatory reaction related to the presence of a foreign body in the defect area (**Figure 4I-L**).

In the G3 group, discreet periosteal bone formation was found at the interface of the defect edge and the outer surface of the composite, showing osteocytes inside and osteoblasts (P<0.05 compared to G2 group, **Figure 6**) on

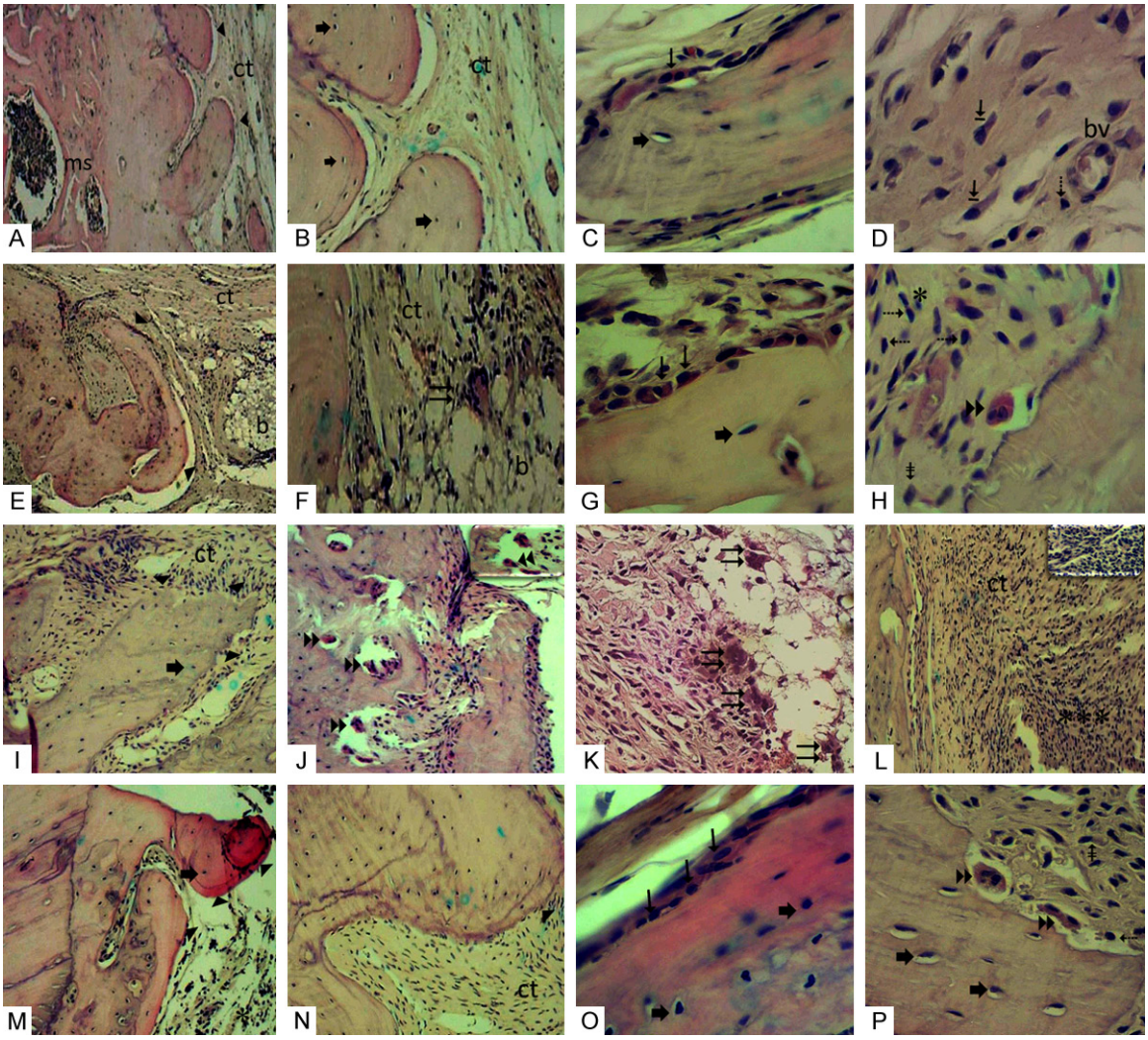

Figure 4. (A-D) G0 Group: (A) Edge of defect exhibiting discreet projection-like bone ▸ formations and medullary spaces (ms). (B) Bone formation with osteocytes ➡ in their gaps and adjacent area filled with collagenized fibrous connective tissue (ct). (C) Bone trabeculae displaying osteoblasts → superficially and osteocytes ➡ within. (D) Collagenized fibrous connective tissue from the defect area, displaying numerous large fibroblasts ↦, lymphocyte ⇢ and BMDblood vessel (bv). (E-H) G1 Group: (E) Bone projections ▸ formed on margin of defect. Connective tissue in defect area (ct) showing remnant intertwining of implanted biomaterial (b). (F) Area showing remnant of implanted biomaterial (b) where multinucleated giant cell ⇉ can be visualized in contact with the periphery of the biomaterial. (G) Bone trabeculae surface showing osteoblastic → paving and osteocytes ➡ inside. (H) Another field in a defect region showing osteoclast ⏵⏵ on bone trabeculae surface and scarce mononuclear inflammatory cells *, lymphocytes ⇢, macrophages ‡. (I-L) G2 Group: (I) Margin of defect showing bone fragments ▸ with irregular margins containing osteocytes ➡. (J) Field showing bone trabecula resorbed by numerous osteoclasts ⏵⏵. In detail, osteoclasts on bone surface. (K) Numerous multinucleated giant cells ⇉ in proximity to the implanted biomaterial. (L) Defect area showing intense inflammatory infiltrate *** permeating collagenized fibrous connective tissue (ct). In detail numerous mononuclear inflammatory cells are observed. (M-P) G3 Group: (M) Bone projections ▸ at the interface of the remnant bone edge and defect displaying osteocytes ➡ inside, scarce scattered inflammatory cells *. (N) Bone fragment ▸ surrounded by collagenized and well-cellularized fibrous connective tissue (ct). (O) Bone fragment presenting osteoblasts → in the periphery and osteocytes ➡ in the interior. (P) In the field near the edge of the defect, osteoclasts ⏵⏵ are sometimes housed in gaps promoting bone resorption, lymphocytes ⇢ macrophages ‡. G0 Group: Positive control critical defect (D) filled with blood clot; G1 Group: Critical defect filled with Hydroxyapatite (H) scaffold; G2 Group: Critical defect filled with zirconia (YSZ) scaffold; G3 Group: Critical defect filled with zirconia/hydroxyapatite (80/20) scaffold. (A, E, I-M) (HE 100 ×); (B, F, N) (HE 200 ×). (C, D, G, H, O, P) details (HE 400 ×).

the periphery, well-cellularized and collagenized fibrous connective tissue, with few mononuclear inflammatory cells ($P<0.01$ compared to G2 group, **Figure 6**) were observed in the

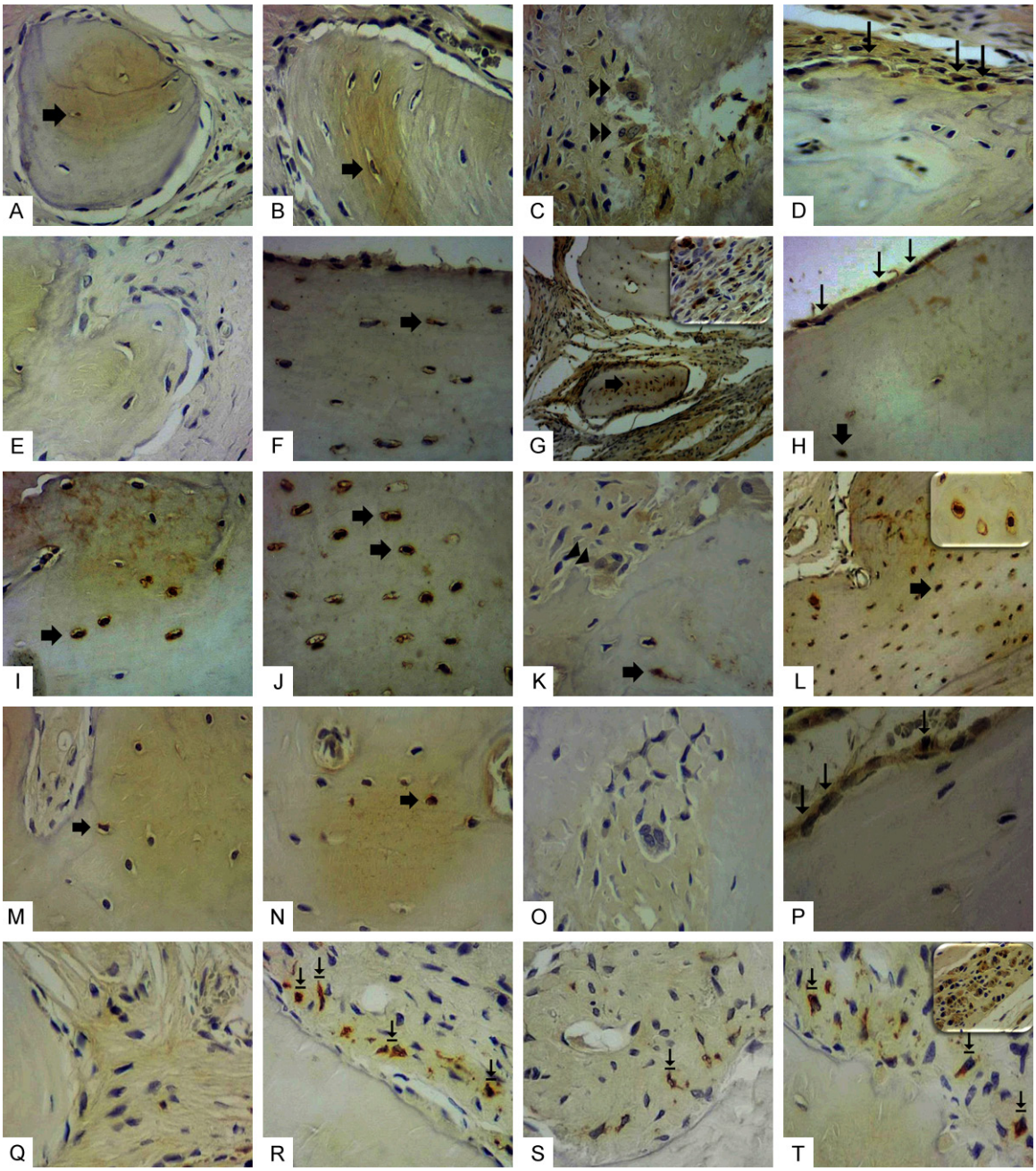

Figure 5. Immunostaining for RANK, RANKL, OPG, OST and FGF-2. (A-D) RANK: presented mild cellular immunostaining in all groups. (E-H) RANKL: (E) Absence of immunostaining in the G0 Group; (F) Weak immunostaining in G1 Group. (G) Intense immunostaining in G2 Group. Detail showing intense mononuclear inflammatory cell marking. (H) Intense immunostaining in G3 Group. (I-L) OPG: intense immunostaining in G0 Group (I) and G1 Group (J); mild in G2 Group (K) and intense in G3 (L). Detail showing intense immunostaining in osteocytes. (M-P) OST: presented moderate immunostaining in G1 Group (N) and G3 Group (P). Mild in G0 Group (M) and absent in G2 (O). (Q-T) FGF-2: no marking in G0 Group (Q); intense immunostaining in fibroblasts near the bone margin in G1 Group (R) and G3 Group (T). In detail (T), another field of the G3 Group exhibiting intense immunostaining in numerous large fibroblasts. G2 Group presented mild immunostaining in fibroblasts (S). Immunostaining in osteocytes (broad arrow), osteoblasts (narrow arrow) osteoclasts (double arrow). G0 Group: Positive control critical defect (D) filled with blood clot; G1 Group: Critical defect filled with Hydroxyapatite (H) scaffold; G2 Group: Critical defect filled with Zircônia (YSZ) scaffold; G3 Group: Critical defect filled with zirconia/hydroxyapatite (80/20) scaffold. LSAB, 400 ×.

central region of the defect. Osteoclasts ($P< 0.05$ compared to G2 group, **Figure 6**) are sometimes found in gaps in fields near the margin, promoting bone resorption (**Figure 4M-P**).

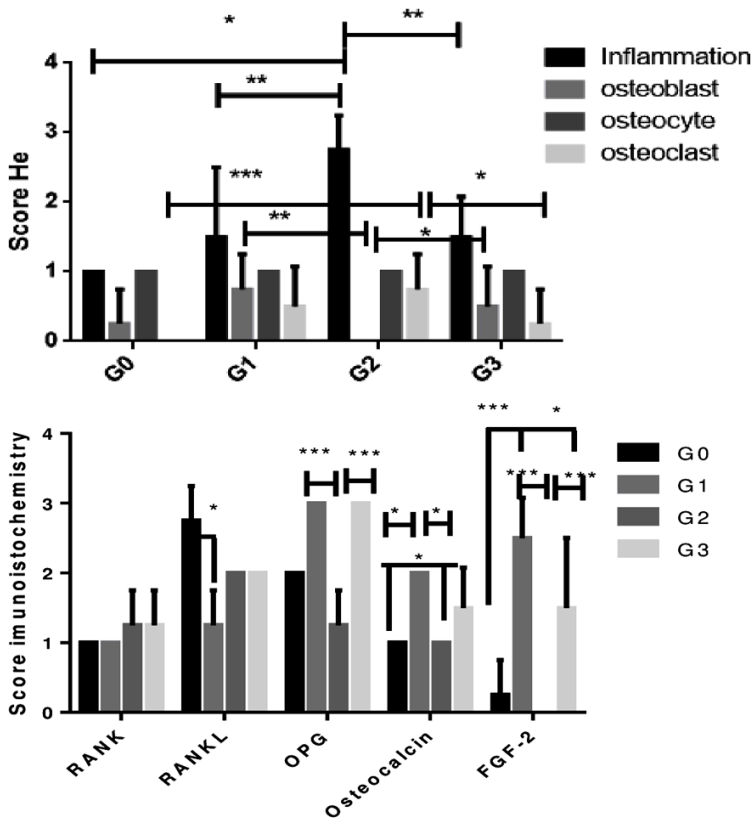

Figure 6. HE score and immunohistochemistry score. G0 Group: positive control (defective and untreated); G1 Group: hydroxyapatite-treated group; G2 Group: Zirconia-treated group; G3 Group: 80/20 Zirconia/hydroxyapatite-treated group (Kruskal-Wallis test followed by Dunn test), (*P<0.05), (***P<0.001), (**P<0.01).

Immunohistochemistry

Immunostaining analysis for RANK, RANKL, OPG, Osteocalcin and FGF-2 was performed in the vicinity of the defect. Weak immunostaining for RANK was observed for all groups. Immunostaining for RANKL was intense for G0 compared to G1 group (P<0.05), moderate immunostaining for G2 and G3 groups, and weak for G1 group. Immunostaining for OPG was intense in G1 and G3 groups when compared to the G2 group (P<0.001). Osteocalcin showed moderate immunostaining in G1 and G3 groups when compared to mild labeling in G0 and G2 groups (P<0.05). Immunostaining for FGF-2 varied from intense to moderate for G1 and G3 groups when compared to G0 and G2 (P<0.05). Immunostaining in connective tissue was detected in mononuclear inflammatory cells and fibroblasts. The type of cellular immunoreactivity was cytoplasmic and nuclear (**Figures 5** and **6**).

Cytokines

Analysis of inflammatory cytokines showed a significant reduction of IL-1 beta for G1 and G3 groups when compared to G0 (P<0.05). IL-10 levels were increased in G1 and G3 groups when compared to G0 and G2 (P<0.05). Regarding TNF-alpha levels, there was a significant reduction for G1 group when compared to G0 (P<0.05, **Figure 7**).

Discussion

Intramembranous ossification, one of two types of bone formation, is responsible for the development of flat or laminated bones, especially in the skull. Bone fracture repair consists of a series of phases: inflammation, soft callus formation, hard callus formation and bone remodeling. Mesenchymal progenitor cells are activated during these phases to undertake migration, proliferation and differentiation [17].

Bone fracture of a bone disrupts the local vasculature within the bone tissue itself and at the endosteal and periosteal surfaces in the bone marrow and in the surrounding soft tissues. This results in hematoma formation due to activation of the plasma coagulation cascade and the platelets exposed to the extravascular environment. The fibrin network thus created serves as the first provisional matrix for the influx of inflammatory cells which are attracted by platelet-derived factors, complement fragments, as well as multiple danger signals released from necrotic cells, damaged extracellular matrix and local tissue macrophages. The first inflammatory cells to arrive to the fracture site within the first 24 hours are neutrophils [18].

Cytokines are a group of proteins known to regulate hemopoietic and immune functions, and are also involved in inflammation, angiogenesis, and bone and cartilage metabolism. All of

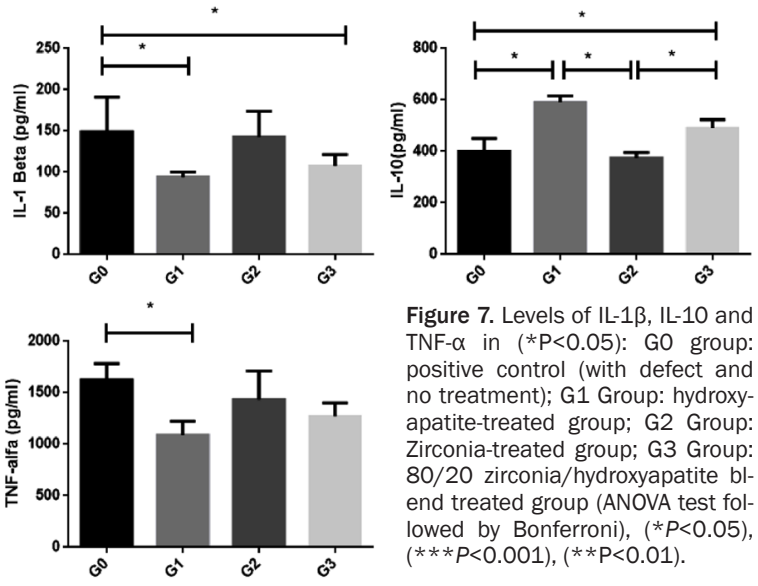

Figure 7. Levels of IL-1β, IL-10 and TNF-α in (*P<0.05): G0 group: positive control (with defect and no treatment); G1 Group: hydroxyapatite-treated group; G2 Group: Zirconia-treated group; G3 Group: 80/20 zirconia/hydroxyapatite blend treated group (ANOVA test followed by Bonferroni), (*P<0.05), (***P<0.001), (**P<0.01).

these processes occur following bone injury, or are known to contribute to wound repair mechanisms. Interleukin-1 is expressed at very low constitutive levels throughout the period of fracture healing, but can be induced to high activities in the early inflammatory phase (day 3). In fracture healing, monocytes are recruited to the site of injury by IL-1 and TNF-α which activates M1 macrophages. The M2 macrophages initiate an anti-inflammatory response in the later stages of inflammation as they secrete tissue repair signals (IL-10, and others), recruit mesenchymal progenitor cells, induce osteochondral differentiation, and prompt angiogenesis [19]. Our data showed decreased IL-1 beta in the G1 and G3 groups. The TNF-alpha levels were decreased in the G1 group. On the other hand, we found a significant increase in IL-10 levels for G1 and G3 groups.

T-cells and B-cells seem to have cell-signaling roles near the end of the inflammatory phase and again during the mineralization phase [20]. T-cells produce RANKL during later stages of the inflammatory phase to recruit, differentiate, and activate osteoclasts, while B cells are involved in suppression of the TNF-α pro-inflammatory signals and produce OPG, thereby regulating osteoblast and osteoclastic differentiation and activity [21].

Our study showed the presence of lymphocyte cells with weak and moderate immunostaining of RANKL in G1 and G3 groups, respectively, but with strong OPG immunostaining in G1 and G3 groups. These represent metabolic bone activity under fracture, with a prevalence of osteoblast cells.

Osteocalcin is an osteoblast-specific protein, and contains three-carboxyglutamic acid residues which provide it with calcium-binding properties. Osteocalcin has been suggested to participate in regulating hydroxyapatite crystal growth. Osteocalcin levels in plasma depend on the formation of new bone, and the concentration may be an indicator of the activity of osteoblasts [22]. Our study showed an increase of osteocalcin in the G1 and G3 groups.

All biomaterials elicit cellular and tissue responses when implanted *in vivo*. These responses include the inflammatory and wound healing responses, foreign body reactions, and fibrous encapsulation of the implanted materials. Macrophages are myeloid immune cells which are tactically situated throughout the tissues, where they ingest and degrade dead cells and foreign materials, in addition to orchestrating inflammatory processes. Macrophages and their fused morphologic variants, the multinucleated giant cells, which include the foreign body giant cells (FBGCs), are the dominant early responders to biomaterial implantation. The foreign body reaction may impact biocompatibility of implantation devices and may considerably impact short- and long-term success in tissue engineering and regenerative medicine, necessitating a clear understanding of the foreign body reaction to different implantation materials [23].

FGF-2 regulates the expression of several molecules [24]. The basic fibroblast growth factor (bFGF) regulate the proliferation of osteoblast-like cells. Cells which migrated from central bone explants of fetal calf calvaria expressed markers which are characteristic of the osteoblast phenotype, including osteocalcin (bone Gla protein) secretion and increased cAMP production in response to treatment with PTH. Bone cells proliferated in response to bFGF in a dose- and time dependent pattern [25].

Nano-Hydroxyapatite (nHAp) is naturally produced by mineralizing cells during bone forma-

tion and remodeling and is the main constituent of the skeleton. nHAp acts as an external stimulus capable of generating specific changes in the expression of a range of genes in osteoblast lineage cells. Understanding the mechanisms by which osteoblast-like cells recognize and respond to the generation of HAp in the extracellular environment is relevant to understanding the process of functional mineralization required for bone homeostasis. There is a need for two specific HAp sensors in phosphate-transporters and Fgf receptors at the cell surface, as well as the stimulation of specific signaling proteins, Frs2α and Erk1/2, downstream of the membrane proteins. The nHAp enhances the differentiation of osteoblast toward terminally differentiated osteocytes [26]. The presence of Hydroxyapatite in G1 and G3 groups can stimulate proliferation and differentiation of osteoblast (osteocalcin) for action in FGF-2 pathways.

Hydroxyapatite (HAp) with the chemical formula $Ca_5(PO_4)_3OH$ could be an excellent material for bone replacement in surgical procedures for human *bone* tissue *repair*. Reported values for fracture toughness of pure HAp are in the range 0.5-1 MPa.√m, while the corresponding values for cortical bone are found in the range of 2-6 MPa.√m, depending on the direction of applied load [27].

Our work showed molecular characteristics related to hydroxyapatite and zirconia/hydroxyapatite (80/20) scaffolds. We also highlight some macroscopic features seen in the Micro CT analysis. First, hydroxyapatite (G1) and zirconia/hydroxyapatite (80/20) scaffolds (G3) have their edges connected to the bone surface. This can be seen in the sagittal and coronal images for the hydroxyapatite (G1) and zirconia/hydroxyapatite (80/20) scaffold (G3) groups. There was an increase in volume [BV/TV (%)] and bone density (BMD mg/cm^3) in the G3 group, close to the hydroxyapatite group (G1). The low tenacity of hydroxyapatite was comprovate. In G1 group, the hydroxyapatite was found broken (Figure, G1, sagittal and coronal, arrows).

Fracture toughness refers to a material's ability to withstand cracking caused by a shock wave crossing it. Ceramics with low elasticity (high Young's Modulus) do not offer high resistance to mechanical shocks compared to metals. However, there is a type of ceramic preferred for applications where the user requires flexural strength in addition to other mechanical properties: zirconium oxide (or zirconia), and in particular Y-TZP zirconia (yttria-stabilised zirconia) or ATZ [28]. In the G2 group with zirconia Y-TZP (yttria stabilized zirconia), it was possible to see presence of fracture toughness; however, zirconia Y-TZP was unable to bind with bone tissue. Thus, the association zirconia/hydroxyapatite (80/20) scaffold (G3) was able show fracture toughness and bind with bone tissue.

Our study showed that zirconia/hydroxyapatite (80/20) scaffold increased bone density, cell bone osteoblast and osteoclast activity, presence of FGF-2, osteocalcin and OPG immunostaining, and increased IL-10 levels.

Acknowledgements

This study was supported by CAPES-PNPD (*Coordenação de Aperfeiçoamento de Pessoal do Nível Superior*). Capes/Print Number: 88887.363681/2019-00. This study was partly financed by the Coordenação de Aperfeiçoamento de Pessoal de Nível Superior-Brasil (CAPES)-Finance Code 001.

Disclosure of conflict of interest

None.

Address correspondence to: Aurigena Antunes de Araújo, AV. Senador Salgado Filho, S/N, Campus Universitário, Centro de Biociências, Departamento de Biofísica e Farmacologia, UFRN, Natal, RN, CEP 59072-970, Brazil. Tel: (84) 32153419; E-mail: aurigena@ufrnet.br

References

[1] Perez-Sanchez MJ, Ramirez-Glindon E, Lledo-Gil M, Calvo-Guirado JL and Perez-Sanchez C. Biomaterials for bone regeneration. Med Oral Patol Oral Cir Bucal 2010; 15: E517-E522.

[2] Habibovic P and de Groot K. Osteoinductive biomaterials--properties and relevance in bone repair. J Tissue Eng Regen Med 2007; 1: 25-32.

[3] Stevens MM. Biomaterials for bone tissue engineering. Materials Today 2008; 11: 18-25.

[4] Huggins RJ and Mendelson BC. Biologic behavior of hydroxyapatite used in facial augmentation. Aesthetic Plast Surg 2017; 41: 179-184.

[5] Wang W and Yeung KWK. Bone grafts and biomaterials substitutes for bone defect repair: a review. Bioact Mater 2017; 2: 224-247.

[6] Nandi SK, Kundu B, Ghosh SK, De DK and Basu D. Efficacy of nano-hydroxyapatite prepared by an aqueous solution combustion technique in healing bone defects of goat. J Vet Sci 2008; 9: 183-191.
[7] El-Ghannam A. Bone reconstruction: from bioceramics to tissue engineering. Expert Rev Med Devices 2005; 2: 87-101.
[8] Liao L, Yang S, Miron RJ, Wei J, Zhang Y and Zhang M. Osteogenic properties of PBLG-g-HA/PLLA nanocomposites. PLoS One 2014; 9: e105876.
[9] Conz MB, Granjeiro JM and Soares Gde A. Hydroxyapatite crystallinity does not affect the repair of critical size bone defects. J Appl Oral Sci 2011; 19: 337-42.
[10] Piconi C and Maccauro G. Zirconia as a ceramic biomaterial. Biomaterials 1999; 20: 1-25.
[11] Brundle CR, Evans CA and Wilson S. Encyclopedia of materials characterization-surfaces, interfaces, thin films. New York: 1992.
[12] Kilkenny C, Browne W, Cuthill IC, Emerson M and Altman DG; NC3Rs Reporting Guidelines Working Group. Animal research: reporting in vivo experiments: the ARRIVE guidelines. Br J Pharmacol 2010; 160: 1577-1579.
[13] Cheng N, Park J, Olson J, Kwon T, Lee D, Lim R, Ha S, Kim R, Zhang X, Ting K, Tetradis S and Hong C. Effects of bisphosphonate administration on cleft bone graft in a rat model. Cleft Palate Craniofac J 2017; 54: 687-698.
[14] Pretel H, Lizarelli RF and Ramalho LT. Effect of low-level laser therapy on bone repair: histological study in rats. Lasers Surg Med 2007; 39: 788-796.
[15] Meurer RT, Martins DT, Hilbig A, Ribeiro Mde C, Roehe AV, Barbosa-Coutinho LM and Fernandes Mda C. Immunohistochemical expression of markers Ki-67, neun, synaptophysin, p53 and HER2 in medulloblastoma and its correlation with clinicopathological parameters. Arq Neuropsiquiatr 2008; 66: 385-90.
[16] Safieh-Garabedian B, Poole S, Allchorne A, Winter J and Woolf CJ. Contribution of interleukin-1 beta to the inflammation-induced increase in nerve growth factor levels and inflammatory hyperalgesia. Br J Pharmacol 1995; 115: 1265-1275.
[17] Egawa S, Miura S, Yokoyama H, Endo T and Tamura K. Growth and differentiation of a long bone in limb development, repair and regeneration. Dev Growth Differ 2014; 56: 410-424.
[18] Loi F, Córdova LA, Pajarinen J, Lin TH, Yao Z and Goodman SB. Inflammation, fracture and bone repair. Bone 2016; 86: 119-130.
[19] Baht GS, Vi L and Alman BA. The role of the immune cells in fracture healing. Curr Osteoporos Rep 2018; 16: 138-145.
[20] Konnecke I, Serra A, El Khassawna T, Schlundt C, Schell H, Hauser A, Ellinghaus A, Volk HD, Radbruch A, Duda GN and Schmidt-Bleek K. T and B cells participate in bone repair by infiltrating the fracture callus in a two-wave fashion. Bone 2014; 64: 155-165.
[21] Pacifici R. T cells, osteoblasts, and osteocytes: interacting lineages key for the bone anabolic and catabolic activities of parathyroid hormone. Ann N Y Acad Sci 2016; 1364: 11-24.
[22] Lowry J. Bone regeneration and repair: biology and clinical applications. Ann R Coll Surg Engl 2006; 88: 334-334.
[23] Sheikh Z, Brooks PJ, Barzilay O, Fine N and Glogauer M. Macrophages, foreign body giant cells and their response to implantable biomaterials. Materials (Basel) 2015; 8: 5671-5701.
[24] Bikfalvi A, Klein S, Pintucci G and Rifkin DB. Biological roles of fibroblast growth factor-2. Endocr Rev 1997; 18: 26-45.
[25] Globus RK, Patterson-Buckendahl P and Gospodarowicz D. Regulation of bovine bone cell proliferation by fibroblast growth factor and transforming growth factor β. Endocrinology 1988; 123: 98-105.
[26] Ha SW, Park J, Habib MM and Beck GR. Nanohydroxyapatite stimulation of gene expression requires fgf receptor, phosphate transporter, and Erk1/2 signaling. ACS Appl Mater Interfaces 2017; 9: 39185-39196.
[27] Ruiz-Ortega M, Esteban V, Suzuki Y, Ruperez M, Mezzano S, Ardiles L, Justo P, Ortiz A and Egido J. Renal expression of angiotensin type 2 (AT2) receptors during kidney damage. Kidney Int Suppl 2003; S21-6.
[28] Marinis A, Aquilino SA, Lund PS, Gratton DG, Stanford CM, Diaz-Arnold AM and Qian F. Fracture toughness of yttria-stabilized zirconia sintered in conventional and microwave ovens. J Prosthet Dent 2013; 109: 165-171.